Chalcogenide Letters Vol. 22, No. 4, April 2025, p. 441 - 450

Electrical properties of Bi_xSe_{100-x} chalcogenide glass

A. Z. Mahmoud [a,b], L. G. Amin [c,*], S. A. Mahmoud [d], M. M. Bashier [e], M. E. M. Eisa [c], N. Dhahri [c], A. Mohamed [e], A. A. Al-Dumiri [c], S. E. I. Yagoub [c], M. A. Abdel-Rahim [b]

[a] *Department of Physics, College of Sciences, Qassim University, Buraydah Almolaydah, 51452, Buraydah, Saudi Arabia*

[b] *Department of Physics, Faculty of Sciences, Assiut University, Assiut 71516, Egypt*

[c] *Physics Department, Faculty of Science, Northern Border University, Arar, Saudi Arabia*

[d] *Center for Scientific Research and Entrepreneurship, Northern Border University, Arar 73213, Saudi Arabia*

[e] *Department of Mathematics, Faculty of Science, Northern Border University, Arar, Saudi Arabia*

The electrical and structural characteristics of Bi_xSe_{100-x} glasses (where x=5, 10, 15, and 25 at. %) were systematically investigated. Using the traditional Quenching of melts process, the amorphous Bi_xSe_{100-x} materials were created. Thin films of Bi_xSe_{100-x} have formed onto ultrasonically glass substrates that have been cleaned using thermal evaporation in a vacuum of approximately 10^-5 Torr. Here we show and discuss the results of four bulk glasses of Bi_xSe_{100-x} (where x=5, 10, 15, and 25 at. %) that were subjected to differential thermal analysis (DTA) under non-isothermal conditions. For the compositions under consideration, five separate methods were used to calculate the activations of the change from amorphous to crystalline. The crystalline phases obtained from differential thermal analysis (DTA), additionally, scanning electron microscopy (SEM) have been characterized utilizing x-ray diffraction. The glass forming factors kg are derived for the analyzed compositions. The relationship between electrical conductivity (σ) and composition, as well as annealing temperature (T) within the range of 300–400 K, has been examined for Bi_xSe_{100-x} (x=5, 10, 15, and 25 at. %) amorphous thin films. The electrical measurements acquired are ultimately analyzed in relation to the amorphous–crystalline change.

(Received January 7, 2025; Accepted April 30, 2025)

Keywords: Conductivity, Amorphous, Electrical properties, Thin film, Hopping distance

1. Introduction

Infrared optical components, fibers, and transmission are all areas where chalcogenide glasses have shown promise [1, 3]. Furthermore, they have been employed in xerography [4], photolithography [6], Memory and switching devices [5], the manufacturing of affordable solar cells [7], and, more lately, in reversible phase shift optical storage [8–11].

Optical recording is currently seen as a viable alternative to magnetic recording. This is attributable not only to the increased information density per unit area on the optical media surface but also to the elimination of head collisions, wear, and dust-related issues associated with magnetic recording. Erasable optical recording is an emerging technique among various optical recording methods, facilitating high-density data storage. The two distinct applications employed in erasable optical recording are magneto-optic and phase-change [10].

Numerous amorphous semiconducting glasses demonstrate a distinctive characteristic of reversible transition [12]. Because of this quality, these spectacles are ideal for use in optical memory systems. At present, phase-change optical recording uses chalcogenide thin films as its recording medium. The films need to possess a great contrast in their optical properties. between their amorphous and crystalline phases and be easily morphable and crystallizable. The transition

*Corresponding author: lamia2014eg@yahoo.com
https://doi.org/10.15251/CL.2025.224.441

between amorphous and crystalline forms can be achieved utilizing the thermal energy of a concentrated laser beam. Significant reflectance disparities between amorphous and crystalline states are utilized for information storage and retrieval. Moreover, the writing and erasing processes must be rapid, and the material should exhibit stability over a sufficient number of write-and-erase cycles while possessing excellent oxidation resistance [11].

Recent investigations have explored the effects of optical memory in amorphous semiconductors for diverse applications [10, 11]. The authors of these studies have documented the application of these films for amorphous-to-crystalline phase transition-based reversible optical recording. They also highlighted the potential of chalcogenide glasses to store both the intensity and phase of illumination due to variations in refractive index caused by light exposure. This is essential for building varied integrated optics and storing holographic optical data.

2. Experimental techniques

Melting quenching approach was used to produce the bulk chalcogenide glasses of the Bi_xSe_{100-x} system (x=5, 10, 15, and 25 at. %). After being measured in accordance with their atomic percentages, the 99.99% pure bismuth (Bi) and selenium (Se) were placed in an evacuated silicon tube. To ensure that all components had a chance to react, the tubes were heated up to 900 °C in stages. The tubes were kept at their highest temperature for a duration of fifteen hours. It was necessary to stir the tube frequently while it melted in order to mix the ingredients and make the liquid more homogeneous. The quenching occurred in an ice water mixture subsequent to this treatment. The alloys were extracted by severing the tube. The amorphous characteristics of the samples that had been created were validated using x-ray diffraction analysis.

2.1. Preparation of thin films

The cleaned glass substrates were coated with thin films of Bi_xSe_{100-x} chalcogenide glasses using the thermal evaporation process. The coating was applied at a pressure of 10^{-5} Torr using the standard Edward E 306 coating machine. Throughout the process of evaporation, the glass substrates were maintained at ambient temperature. Evaporation was accomplished using a molybdenum boat. An Edward FTM5 quartz crystal monitor was employed to regulate the evaporation rates and film thicknesses that were studied. To deposit all the necessary films, an evaporation rate of 2.5 nm s^{-1} was kept up. In order to ensure uniform and homogeneous deposition, the substrate holder was rotated throughout the evaporation process.

3. Results and discussion

3.1. X-ray diffraction (XRD)

The X-ray examination of the thin films that are both annealed and unannealed that were placed on glass substrates was conducted using a Philips model PW1710 X-ray diffractometer. This diffractometer had a Ni-filtered Cu K source (λ =1.542) that was run at 40 kV, 30 mA, and 3.7 degrees per minute of scanning speed. Conversely, we compare the d-space of the apparent peaks with ASTM cards to determine the crystallographic phases that occurred in the XRD patterns of the annealed films.

3.2. Electrical measurements

In this section, the procedure for determining the films' electrical resistance, both as-prepared and after annealing, in relation to temperature is described in detail. Following the cleaning of the glass substrate, a 300 nm film was applied. Two planar electrodes made of aluminum were then placed onto the films employing a thermal evaporation method in a 10^{-5} Torr vacuum. The process was illustrated in Figure (1).

A traditional circuit utilizing a Keithley 610C electrometer was utilized to determine the electrical resistance value. All of these readings were taken between 300 and 400 K in complete darkness.

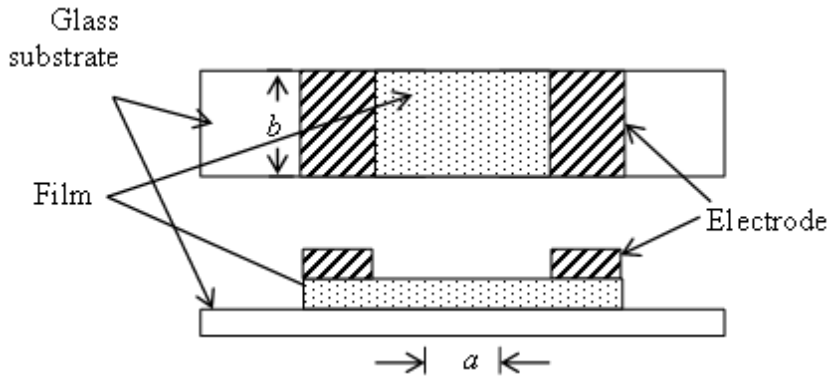

Fig. 1. Method of thermally evaporating in a 10^{-5} Torr vacuum.

The electrical resistance value (R) of the sample is calculated by using the equation that follows:

$$R = \rho a / db \tag{1}$$

where ρ is the resistivity of the sample, a is the distance between the electrode (a = 2 mm), The electrodes' length is denoted by b, and the film's thickness by d. By measuring the resistance R, we can obtain the resistivity from the above equation.

3.3. SEM examination of annealed Bi-Se films

Scanning Electron Microscope (SEM) analysis helps one investigate the shape of the materials following annealing to crystallization temperature. Before SEM analysis, the sample is broken and gold covered in order to investigate internal shape as well as surface. Fig. 2 (a, b, c and d) shows scanning micrographs of samples with different compositions that were annealed for an hour at 383 K.

Figure (2-a) shows the surface microstructure of Bi_5Se_{95}. There is polycrystalline structure shown in the photomicrograph. Embedded in amorphous matrix, the polycrystalline structure comprises of crystallites. The fact that the crystallization is just in its first phases makes the crystalline form not distinguishable. Figure (2-b) shows the resulting microstructure for the annealed composition $Bi_{10}Se_{90}$. Solidification has not yet occurred in most of the structure, which is mostly amorphous. The concentration of Bi increases the size of the crystallites. The annealed microstructure that was produced $Bi_{15}Se_{85}$ composition is shown in Figure (2-c), and the polycrystalline structure is clearly discernible. Contained inside an amorphous matrix are many crystalline phases of varying shapes and sizes. The crystallites disperse in an amorphous matrix in a manner that is not uniform, as previously mentioned. The annealed sample's electron scanning micrograph $Bi_{25}Se_{75}$ material, on the other hand, shows that there is amorphous matrix with several crystalline phases incorporated in it in the surface microstructure. The majority of the structure is taken up by crystallites, as seen in Figure (2-d) due to the fact that certain crystalline particles are isolated, while others are connected.

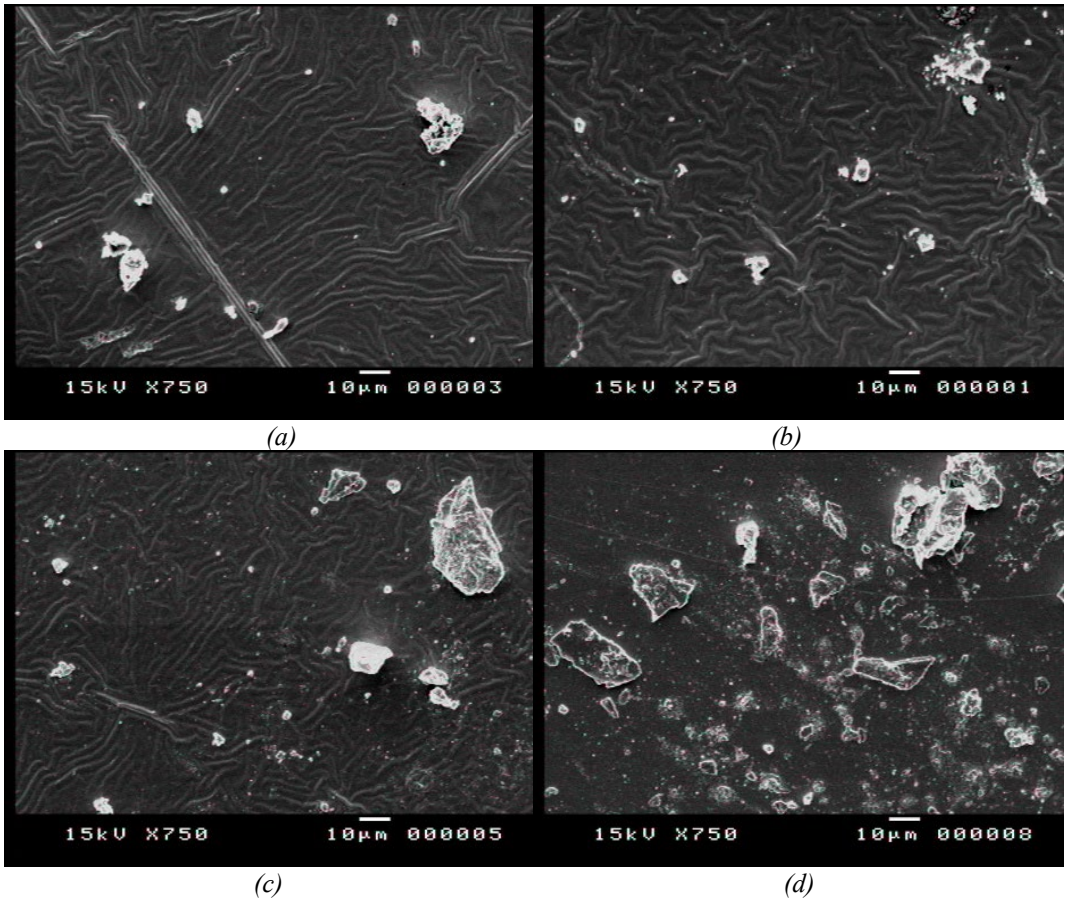

Fig. 2. Photograph of SEM for specimens of various annealed compositions at 383 K for 1 h (a) Bi_5Se_{95} (b) $Bi_{10}Se_{95}$ (c) $Bi_{15}Se_{85}$ (d) $Bi_{25}Se_{75}$.

3.4. X-ray examination of annealed Bi-Se films

The patterns of x-ray diffraction are analyzed to identify the phases of crystals observed in the SEM examination. The examination has been conducted on specimens that were annealed at temperatures near the crystallization point, as illustrated in Fig. (3). The initial alloy composition determines the crystallization phases. The x-ray diffraction pattern analysis illustrates that the Bi_2Se_3 and Se phases are responsible for the crystalline peaks that were found, as shown in Figure (3).

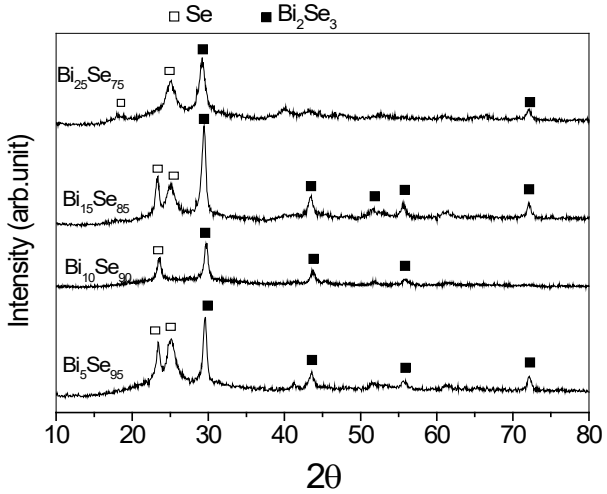

Fig. 3. X-ray diffraction pattern for the Bi_xSe_{100-x} (x=5, 10, 15, and 25 at. %) annealed at 383 K for 1 h.

4. Effect of composition on the electrical properties

"The temperature dependence of the direct current electrical conductivity" (σ) has been investigated for the as-prepared Bi_xSe_{100-x} (x=5, 10, 15, and 25 at. %) films. The measurements were conducted on films with a thickness of 300 nm, The substrates were made of glass and kept at the ambient temperature. After the sample had been heated to 400 K from room temperature, the electrical resistance was measured. Figure 4 illustrates the ln(σ) versus 1000/T curves for the as-deposited Bi_xSe_{100-x} films. The electrical conductivity curves exhibited two distinct regions: one corresponding to hopping conduction and the other associated with conduction through extended states. Below "the glass transition temperature", "the electrical conductivity" (σ) exhibits a modest increase with rising temperature, which is associated with transport via hopping conduction. Conversely, at temperatures exceeding T_g, the electrical conductivity (σ) exhibits an exponential increase with temperature (T). This increase can be considered as typical extended-state band-type conduction.

Generally, the calculated conductivity is thought to be the sum of two elements [13]:

$$\sigma = \sigma_{hop} + \sigma_{ext} \tag{2}$$

where σ_{hop} is "the contribution of conduction due to hopping between the localized states" and σ_{ext} is "the contribution of conduction between the extended states".

When there is a dense enough population of localized states, this hopping mechanism can take place. [14, 15].

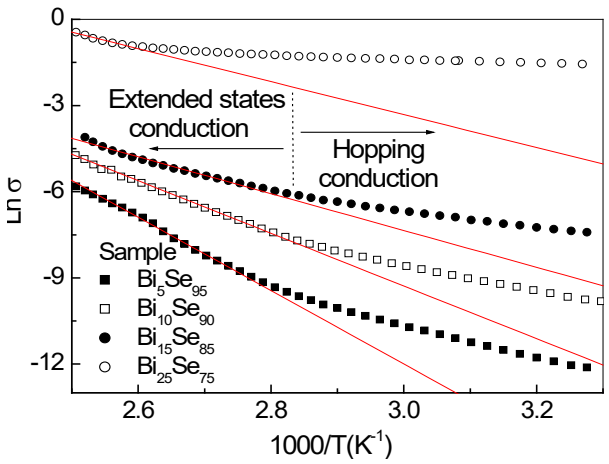

Fig. 4. Plots of ln σ versus 1000/T for the Bi_xSe_{100-x} films.

When the temperature is low (300 K < T ≤ 350 K), Carriers of charge at the Fermi level in confined states engage in variable-range hopping, allowing conduction to occur. According to Mott's relation [13, 16], the conduction in this area is defined as:

$$\sigma = (\sigma_o / \sqrt{T}) \exp(-(T_o / T)^{1/4}) \tag{3}$$

with

$$T_0 = 18\alpha^3 \lambda / k_B N(E_f) \tag{4}$$

where T_o is "the degree of disorder", $N(E_f)$ is "the density of localized states at the Fermi level", k_B is "the Boltzman constant", λ is "a dimensionless constant" and α is "the coefficient of the

exponential decay of the localized state wave function" (i.e. α^{-1} represents the degree of localization). The coefficient α is assumed to be 0.125 Å^{-1} [17].

Figure 5 illustrates the linear graphs of ln (σ_{hop} $T^{1/2}$) vs $(1/T)^{1/4}$ for the examined compositions. The slopes of the resultant straight lines were utilized to compute the values of T_o, which are presented in Table (1). Table 1 displays the computed density of localized states at the Fermi level, $N(E_f)$, for the compositions that were taken into consideration. As the Bi content increases from 5 to 25 atomic percent, Figure 6 shows that $N(E_f)$, the density of localized states, increases.

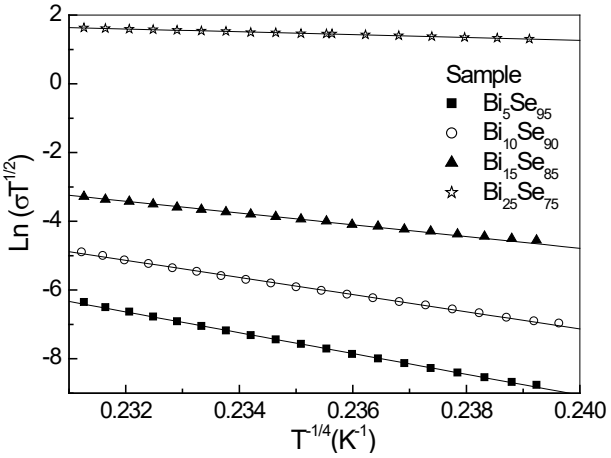

Fig. 5. ln (σ $T^{1/2}$) versus $T^{-1/4}$ plots for the Bi_xSe_{100-x} films.

"The hopping distance" R (cm) and "the hopping energy" W (eV) are two additional hopping parameters that can be determined, as stated by Mott [18] and Davis et. al. [19]. The two variables are defined as follows:

$$R = \left[\frac{9}{8\pi k_B T N(E_f)}\right]^{1/4} \tag{5}$$

$$W = \frac{3}{4\pi R^3 N(E_f)} \tag{6}$$

Table (1) displays the values of R and W which calculated for the experimental films. Figure 6 illustrates the reduction of the average hopping energy Was the Bi concentration increases. The findings of $N(E_f)$ and W concur with those of Majeed Khan et al. [20].

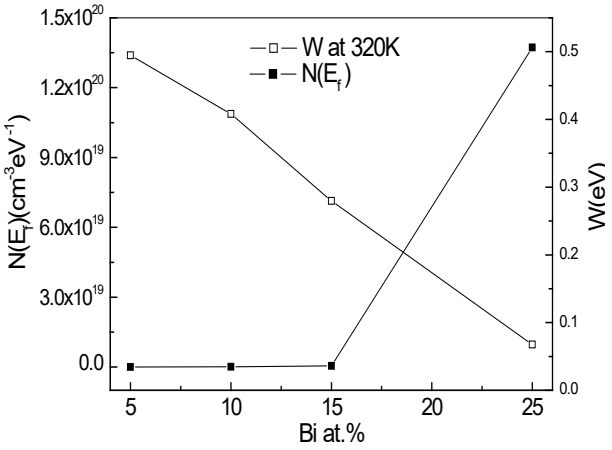

Fig. 6. The relationship between the Bi content in the studied films and the average hopping energy, W, and the density of localized states at the Fermi level, N(Ef).

Table (1) indicates that as a concentration of Bi rises, the values of W and to fall. Because of the degree of disorder and the degree of localization, and the amorphicity of the samples diminishes as the concentration of Bi rises.

Table 1. Composition matters for the as-deposited Bi_xSe_{100-x} films in terms of DC conductivity, disorder degree, hopping distance, hopping energy, The density of Fermi-level localization and energy of activation.

Comp.	ΔE (eV)	σ ($\Omega^{-1}cm^{-1}$)	T_o (K)	$N(E_f)$ ($cm^{-3}eV^{-1}$)	R(cm) At320K	W (eV) At 320K
Bi_5Se_{95}	1.10	1.22×10^{-4}	8.40×10^{9}	4.74×10^{16}	2.17×10^{-6}	0.50
$Bi_{10}Se_{90}$	0.79	6.86×10^{-4}	3.89×10^{9}	1.02×10^{17}	1.79×10^{-6}	0.41
$Bi_{15}Se_{85}$	0.55	0.00317	8.57×10^{8}	4.64×10^{17}	1.23×10^{-6}	0.28
$Bi_{25}Se_{75}$	0.49	0.271	2.90×10^{6}	1.37×10^{20}	2.96×10^{-7}	0.07

Charged impurities in the Bi-Se bond structure are responsible for the observed increase of $N(E_f)$ with increasing Bi concentration. The introduction of Bi results in the creation of three ions, one of which is positively coordinated and the other negatively charged [21]. The balance between the negatively charged D^- bonds and the positively charged D^+ dangling bonds is thought to be the reason why the Fermi energy is fixed to the middle of the band gap [21]. The entry of the impurity must upset the equilibrium and cause the unplugging of the Fermi energy, which is connected to an increase in the density of localized states [20].

Conversely, a great deal of systemic faults is introduced when B_i is added since it enhances the Bi-Se bonds. The concentration of the Bi-Se bond grows as the B_i content does, but the link between chalcogen atoms, like Se-Se, grows weaker. As a result of this process, the value of the localized state density rises.

In high temperature region, Figure (4) illustrates the relationship between ln (σ) and 1000/T, which shows that σ(T) behaves exponentially and may be explained by the Arrhenius relation:

$$\sigma = \sigma_o \exp(-\Delta E / k_B T) \tag{7}$$

where ΔE is "the activation energy" for DC conduction, k_B is "the Boltzmann constant" and σ_o is "the pre-exponential factor". The ΔE values are calculated from the slope of straight lines of Eq. (7) and listed in Table (1).

The electrical conductivity (σ) measured at ambient temperature (T = 307.35 K) and the calculated energy of activation for DC conduction (ΔE) are shown in Figs. (7) and (8). The two parameters have exactly opposite manner change with composition. The values of (ΔE) decrease while the values of (σ) increase with increasing Bi content. That the change in (σ) is linked to a similar change in (ΔE) is confirmed by this.

Approximately half of the optical energy gap's magnitude is determined by the computed values of (ΔE). E_f is thus quite close to the mobility gap's center.

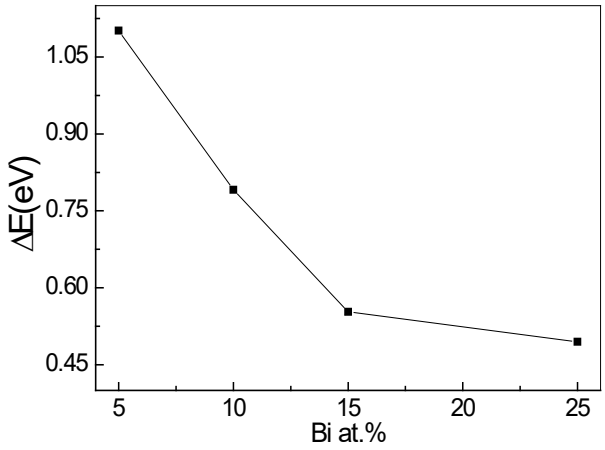

Fig. 7. The relationship between the activation energy and the Bi content of the films under investigation.

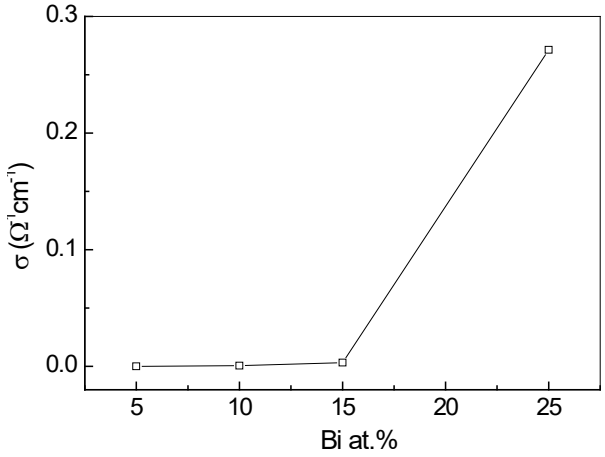

Fig. 8. The relationship between DC conductivity and the Bi content of the study films.

This variation in activation energy and DC conductivity for 9 at. % Bi was seen in both the SeGeBi [22] and SeGeTeBi [23] alloys. A rise in conductivity of direct current and a decrease in activation energy are observed in chalcogenide glasses doped with impurities, which is associated with a shift in the Fermi level [24, 25]. The metallic nature of bismuth is largely responsible for this behavior. Adding Bi to a chalcogenide matrix makes it behave like a metal, which unpins the Fermi level, moves it into the conduction band, and changes it to n-type conduction [26].

One possible explanation for the enhanced conductivity is the presence of impurity atoms, which could lead to an increase in hopping conduction [25]. Conduction can occur in the localized states via hopping or above the mobility edge in the extended states.

5. Conclusion

Following characteristics are highlighted by the current experiment on the Bi_xSe_{100-x} glassy system (x = 5, 10, 15, and 25 at. %): Every composition exhibits a single stage of crystallization with a single glass transition. Findings showed that composition had an effect on T_g's and E_g's. It was discovered that the composition depends on the parameters of crystallization T_c, T_p, k_o, k_p, k_g, and E_c. The findings show that the Bi_xSe_{100-x} crystallization process follows an Avrami exponent (n)-dependent one- and two-dimensional growth mechanism. As the Bi concentration increases, the glass forming ability (GFA) decreases, according to the frequency factor, glass formation factor, and anticipated crystallization activation energy. Two transitions with two energy gaps were detected in the optical absorption studies of Bi_xSe_{100-x} thin films, suggesting that the mechanism of absorption is a direct transition.

The existence of a secondary phase is thought to be the source of these characteristics. As the Bi content increases, the as-deposited thin films' optical energy gap E_g shrinks. This is because the bond energy decreases as the Bi concentration increases. During the annealing process of Bi_xSe_{100-x} films, the energy gap widens up until the glass transition temperature (T_g), after which it drops dramatically. After annealing at temperatures greater than T_g, SEM tests revealed that the material undergoes amorphous-crystalline transition. As the γ-irradiation dose increases, the energy gap narrows in the irradiation Bi_xSe_{100-x} films. The observed impact is thought to be associated with atomic disorder and bond rearrangements in the studied amorphous chalcogenide composition. Two different kinds of conduction channels, each contributing one of two different mechanisms, are shown by the electrical results. It was demonstrated that as the Bi concentrations rose, the activation energy for electrical resistivity and conduction at 307.35 K decreased. It was shown that when the temperature of annealing rose, the activation energy of electrical resistance and conduction decreased. The change from amorphous to crystalline is responsible for this.

Conflict of interest

The authors declare that there is no conflict of interest regarding the publication of this paper

References

[1] A. R. Ilibton, D. Haynes, M. Rechtin, J. Non-Cryst. Solids, 17 (1965) 319.
[2] J. R. Ganon, Proc. SPIE 266 (1981) 62; https://doi.org/10.1117/12.959899
[3] E. Marquez, P. Villars, R-G. Jimenez, J. Mater. Res. 3 (1988) 314; https://doi.org/10.1557/JMR.1988.0314
[4] J. H. Dessaur, H. E. Clarke, Xerography and Related Processes. Local, London, 1965.
[5] S. R. Ovshinsky, Phys. Rev. Lett. 21 (1986) 1450; https://doi.org/10.1103/PhysRevLett.21.1450
[6] D. E. Carlson, C. R. Wronski, Appl. Phys. Lett. 28 (1976) 671; https://doi.org/10.1063/1.88617
[7] J. Fusong, M. Okuda, Jpn. J. Appl. Phys. 30 (1991) 97; https://doi.org/10.1143/JJAP.30.97
[8] N. F. Mott, Adv. Phys. 16 (1967) 49; https://doi.org/10.1080/00018736700101265
[9] N. F. Mott, Philos. Mag. 34 (1976) 1101; https://doi.org/10.1080/00318087608227732
[10] L. K. Malhotra, Y. etccc, Bull. Mater. Sci, 18 (1995) 725; https://doi.org/10.1007/BF02744807

[11] K. A. Rubin, M. Chen, Thin Solid Films, 181 (1989) 129; https://doi.org/10.1016/0040-6090(89)90479-3
[12] K. Tanaka, Phys. Rev. B 39 (1989) 1270; https://doi.org/10.1103/PhysRevB.39.1270
[13] N. F. Mott, Philos. Mag. 19 (1969) 835; https://doi.org/10.1080/14786436908216338
[14] A. K. Jonscher, J. Vac. Sci. Technol. 8 (1971) 135; https://doi.org/10.1116/1.1316261
[15] R. D. Gould, B. B. Ismail, Phys. Stat. Sol. (a) 134 (1992) K65; https://doi.org/10.1002/pssa.2211340233
[16] H. Mori, K. Cotoch, H. Sakata, J. Non-Cryst. Solids 183 (1995) 22; https://doi.org/10.1016/0022-3093(94)00585-0
[17] S. Mahadevan, A. Giridhar, K.J. Rao, J. Phys. C 10 (1977) 4499; https://doi.org/10.1088/0022-3719/10/22/019
[18] N. F. Mott, Phil. Mag. 32 (1975) 961; https://doi.org/10.1080/14786437508221667
[19] E. A. Davis, N. F. Mott, Phil. Mag. 22(1970) 903; https://doi.org/10.1080/14786437008221061
[20] M. A. Majeed Khan, M. Zulfequar, M. Husain, Physica B 322 (2002) 1; https://doi.org/10.1016/S0921-4526(01)00640-8
[21] N. F. Mott, E.A. Davis, Electronic Processes in Non-Crystalline materials (1978).
[22] N. Tohge, T. Minami, M. Tanaka, J. Non. Cryst. Solids 37 (1980) 23; https://doi.org/10.1016/0022-3093(80)90475-5
[23] P. Negals, M. Retti, S. Vikrov, J. de Phys. 42 (C 4) (1981) 907;
[24] S. Okano, M. Suzuki, K. Imura, N. Fukada, A. Hiraki, J. Non-Cryst. Solids 59-60 (1983) 969; https://doi.org/10.1016/0022-3093(83)90330-7
[25] B. T. Kolomiets, E. A. Lebedev, N. A. Rogachev, Fiz. Tekh. Popuorov. 8 (1974) 545.
[26] H. Fritsche, P. J. Gaczi and M. A. Kastner, Phil. Mag. B 37 (1978) 593; https://doi.org/10.1080/01418637808226453